# Porcine Sub-Retinal Pigment Epithelium Deposits: A Model for Dry Age-Related Macular Degeneration With Comparison to Human Drusen

Erika M. Shaw,[1] David M. Anderson,[2] Ramesh Periasamy,[3] Kevin L. Schey,[2] Christine A. Curcio,[4] and Daniel M. Lipinski[1,3]

[1]Department of Cell Biology, Neurobiology and Anatomy, Medical College of Wisconsin, Milwaukee, Wisconsin, United States
[2]Department of Biochemistry, Vanderbilt University, Nashville, Tennessee, United States
[3]Department of Ophthalmology and Visual Sciences, Medical College of Wisconsin, Milwaukee, Wisconsin, United States
[4]Department of Ophthalmology and Visual Sciences, University of Alabama at Birmingham Heersink School of Medicine, Birmingham, Alabama, United States

Correspondence: Daniel M. Lipinski, Department of Cell Biology, Neurobiology and Anatomy, Medical College of Wisconsin, 8701 Watertown Plank Rd., Milwaukee, WI 53226, USA; dlipinski@mcw.edu.

**Received:** September 4, 2024
**Accepted:** January 7, 2025
**Published:** March 6, 2025

Citation: Shaw EM, Anderson DM, Periasamy R, Schey KL, Curcio CA, Lipinski DM. Porcine sub-retinal pigment epithelium deposits: A model for dry age-related macular degeneration with comparison to human drusen. *Invest Ophthalmol Vis Sci*. 2025;66(3):18. https://doi.org/10.1167/iovs.66.3.18

**Purpose.** Due to the slowly progressing nature of age-related macular degeneration (AMD) and critical differences in ocular anatomy between humans and animals, it has been difficult to model disease progression, hampering the development of novel therapeutics aimed at impacting drusen biogenesis. To determine whether "drusen-in-a-dish" model systems are of utility in screening potential therapeutics aimed at early–intermediate dry AMD, we developed a detailed characterization of the protein, glycoprotein, and lipid composition of sub-retinal pigment epithelium (RPE) deposits grown by monolayers of ex vivo porcine RPE with human drusen in AMD globes.

**Methods.** Immunohistochemistry and imaging mass spectrometry (IMS) were performed on 20-week aged monolayers of porcine RPE and human donor globes recovered from an 81-year-old non-transplant donor with confirmed diagnosis of bilateral dry AMD. The presence of major protein, glycoprotein, and lipid species was compared between porcine sub-RPE deposits and human drusen with reference to macular/peripheral eccentricity.

**Results.** The protein and glycoprotein composition of porcine sub-RPE deposits closely mimics human drusen identified in donor globes with dry AMD, including the presence of major complement components (C9, CFH, CHI), apolipoproteins (ApoE, ApoJ), extracellular matrix proteins (vitronectin, collagen VI), and calcification (hydroxyapatite). Sub-RPE deposits were additionally rich in long-chain ceramide species (Cer, CerPE, PI), which have only recently been described in human drusen.

**Conclusions.** Due to their compositional similarity to human drusen, ex vivo "drusen-in-a-dish" systems represent a potentially robust and cost-effective model for both studying the pathobiology of drusen biogenesis and screening novel therapeutics aimed at limiting drusen formation.

Keywords: retinal pigment epithelium, age-related macular degeneration, primary RPE, cell culture model, sub-RPE deposits

Age-related macular degeneration (AMD) is a leading cause of visual impairment in the elderly and has been estimated to affect approximately 8.7% of all individuals between the ages of 45 and 85 years.[1,2] The atrophic, or "dry," form of AMD represents approximately 85% to 90% of all cases and clinically is most commonly characterized by the deposition of lipoproteinaceous material beneath the retinal pigment epithelium (RPE) that accumulates to form drusen.[3–6] Although the role that drusen play in the pathogenesis of AMD is complex, the deposited materials are hypothesized to inhibit nutrient and oxygen cycling across Bruch's membrane (BrM)—a multilaminar structure consisting of alternating layers of collagen and laminin that separates the RPE from the underlying choriocapillaris—leading to degeneration of the RPE and overlaying photoreceptors.[7–9] In intermediate- to late-stage dry AMD, degeneration of the RPE and neural retina within the macula and fovea advances, leading to geographic atrophy, and is associated with slowly progressing (i.e., occurring over years or decades) but irreversible loss of central vision.[8,10,11] In approximately 10% to 15% of AMD patients, the disease progresses to an exudative, or "wet," form characterized by the abnormal growth of blood vessels from the choroid extending into the neural retina. This neovascularization occurs most frequently in areas of widespread geographic atrophy where BrM is already severely compromised, leading to rapid (i.e., over a period days or weeks) vision loss primarily due to inflammation caused by edema and

sub-retinal hemorrhaging.[5,6] Although wet AMD is the faster progressing of the two forms, it can be managed effectively through periodic injections of vascular endothelial growth factor (VEGF) inhibitors to limit neovascularization. Dry AMD remains without any effective treatments; however, the only currently approved therapy of dietary supplementation with Age-Related Eye Disease Study (AREDS) vitamins, which include zinc, carotenoids, and antioxidants, may be beneficial in slowing the degeneration of the RPE and photoreceptors.[4,8,12–16]

Due to the important role that drusen deposition likely plays in the development and progression of AMD, and despite the precise mechanism of their accumulation being a subject of widespread debate, their overall composition has been well documented. Although the deposits are variable based on anatomical location and drusen subtype, they are generally comprised of approximately 40% to 60% lipids (e.g., esterified cholesterol, phosphatidylcholine), with the remaining druse volume consisting of various proteins (e.g., apolipoproteins, components of the complement cascade, extracellular matrix and basement membrane proteins) and minerals (e.g., hydroxyapatite).[8,17,18]

Although numerous animal models accurately recapitulate certain aspects of AMD pathology—including the accumulation of sub-RPE deposits and RPE death—all have major limitations that impact their utility for screening the safety and efficacy of novel treatments, such as gene and cell therapies.[4,19–25] The first major limitation facing the use of animals to model AMD is that the hallmark pathologic lesions of disease occur specifically within the macula, a specialized anatomical feature that, with the exception of non-human primates (NHPs), does not exist in the animal species most commonly utilized for research, such as rodents, rabbits, or swine. Second, as AMD is a complex disease with numerous genetic and environmental risk factors contributing to disease progression, no single causative alleles have been identified that could be exploited to generate transgenic animal models with a consistent AMD phenotype.[26–29] Finally, the largest contributor and most predictive risk factor for developing AMD is advanced age, which presents a serious hurdle to modeling disease progression in animals, as small animal species do not live long enough to develop age-related ocular pathologies, and aging-out NHPs is financially and practically prohibitive.[30]

As a consequence of these limitations, there is substantial motivation for the development of alternative strategies to model AMD pathogenesis and screen novel therapeutics aimed at halting or reversing disease progression. In particular, our groups and others have focused on the development of cost-scalable cell culture model systems capable of recapitulating the major pathogenic lesions of AMD, including those derived from human donor tissues, human induced pluripotent stem cells (iPSCs), and animal tissues, all of which offer advantages and limitations. Ideally, human tissues would be used to model dry AMD, and primary human fetal RPE has been shown to develop tight junctions with apical–basolateral polarity when cultured as monolayers on semipermeable membrane supports, with the development of apolipoprotein E (ApoE)-positive sub-RPE deposits that trigger complement system activation occurring within 1 to 3 months.[31–33] Cultures of RPE isolated from adult postmortem tissues have also been used to probe how RPE function is altered (e.g., mitochondrial dysfunction, differential expression of proteins) in AMD versus healthy donor RPE and provides an opportunity to correlate genetic and epigenetic risk variants directly to RPE physiology.[34–40] Unfortunately, in addition to being costly, human RPE is an incredibly scarce resource, especially when required to be derived from donors with a confirmed diagnosis of AMD and within short time scales postmortem to allow for viable cultures, which significantly limits its utility in most laboratories. Human iPSC-derived RPE offers a more abundant option for the use of human tissues for both dry AMD pathology research as well as drug development. Indeed, human iPSC-derived RPE has been used to explore changes in RPE cell morphology and physiology due to variants in genetic loci associated with dry AMD risk (e.g., *CFH*, *ARMS2/HTRA1*), revealing abnormalities in antioxidant defense capacity, mitochondrial function, and complement protein expression and activation.[34,41–43] iPSC-derived RPE cultured from individuals with various complement factor H (CFH) risk alleles has also been used to demonstrate that individuals with high-risk CFH alleles are more likely to develop a dry AMD phenotype typified by the accumulation of sub-RPE deposits and RPE atrophy upon complement stimulation, and they have been used in the identification of two potential new therapeutic agents (L-745, 870) aimed at modulating drusen formation.[34,44] Although these tissues offer a functionally infinite source of human RPE, the process of inducing pluripotency, differentiating iPSCs, and experimentally validating the resultant unique cell lines (e.g., haplobanking, checking for presence of residual episomal vectors) is laborious and time consuming, restricting their use as a model system for mass screening.[45]

The use of primary RPE tissues derived from animals bridges the gap between scarce, costly human tissues and semi-immortalized human-derived cell lines, such as iPSCs. When cultured on semipermeable inserts, primary RPE cells from a variety of animal sources, including NHPs, mice, and pigs, have been documented to develop polarized monolayers with features that mimic RPE in situ, including the formation of sub-RPE deposits containing known components of human drusen (e.g., apolipoproteins, lipids, hypoxyapatite).[46–48] Such findings suggest that these cultures may have value as tools for therapeutic development and especially high-throughput drug screening. Herein, we aimed to expand upon these studies by extensively characterizing a porcine "drusen-in-a-dish" model. Specifically, using a combination of postmortem histology and imaging mass spectrometry (IMS), we aimed to characterize the protein, lipid, and mineral composition of spontaneously occurring sub-RPE deposits in ex vivo cultures of primary porcine RPE, focusing on targets (e.g., complement components, apolipoproteins, neutral lipids) (Table 1) selected based on previous published reports describing the presence of each molecule in human drusen.[8,17,18] Importantly, we compared the composition of laboratory-grown sub-RPE deposits to drusen identified in human donor globes with confirmed diagnoses of AMD, giving particular emphasis to ocular eccentricity, which allowed us to maintain spatial resolution and determine whether "drusen in a dish" are more compositionally similar to specific drusen subtypes involved in AMD progression (e.g., soft macular drusen) than those associated with normal aging (e.g., hard peripheral drusen). As such, this study provides valuable additional characterization of RPE "drusen-in-a-dish" culture models and validates whether they might be utilized for high-throughput, cost-scalable screening of novel therapeutics aimed at preventing

**Table 1.** Antibody, Lectin, and Dye Concentrations, Reactivities, and Sources

| Reagent | Specificity | Figure | Concentration | Reactivity | Supplier | Identifier |
|---|---|---|---|---|---|---|
| Complement factor H (CFH) monoclonal antibody | Complement factor H | 1A–1C | 1:100 | H | Thermo Fisher Scientific | Invitrogen GAU 018-03-03 |
| Complement factor I (CFI) polyclonal antibody | Complement factor I | 1A–1C | 1:100 | H, M, P | Thermo Fisher Scientific | Invitrogen PA5-96371 |
| Complement component 9 (C9) polyclonal antibody | Complement component 9 | 1D–1F | 1:100 | H, M, R | Thermo Fisher Scientific | Invitrogen PA5-29093 |
| Apolipoprotein E (ApoE) polyclonal antibody | Apolipoprotein E | 2A–2C | 1:100 | H, P | Thermo Fisher Scientific | Invitrogen PA5-18361 |
| Apolipoprotein J (ApoJ) polyclonal antibody | Apolipoprotein J | 2D–2F | 1:100 | H, M, P | Thermo Fisher Scientific | Invitrogen PA5-46931 |
| Vitronectin polyclonal antibody | Vitronectin | 3A–3C | 1:100 | H, M, R, P | Thermo Fisher Scientific | Proteintech 15833-1-AP |
| Collagen type VI polyclonal antibody | Collagen VI | 3D–3F | 1:100 | H, P | Thermo Fisher Scientific | Proteintech 14853-1-AP |
| Laminin monoclonal antibody | Laminin 5 | 3D–3F | 1:100 | H, M, P | Thermo Fisher Scientific | Invitrogen MA1-06100 |
| Collagen type IV polyclonal antibody | Collagen IV | 3G–3I | 1:100 | H, M, R, B, mammal | Thermo Fisher Scientific | Invitrogen PA1-28534 |
| Collagen type V polyclonal antibody | Collagen V | 3J–3L | 1:200 | H, B | Thermo Fisher Scientific | Rockland 600-401107-01 |
| *Lens culinaris* agglutinin (LCA)—FITC | Mannose, glucose | 4A–4C | 100 µg/mL | N/A | Thermo Fisher Scientific | Invitrogen L32475 |
| Concanavalin A (ConA)—Alexa Fluor 594 | $\alpha$-Mannopyranosyl, $\alpha$-glucopyranosyl | 4D–4F | 100 µg/mL | N/A | Thermo Fisher Scientific | Invitrogen C11253 |
| *Ricinus communis* agglutinin I (RCA I)—FITC | Galactose, N-acetylgalactosamine | 4G–4I | 200 µg/mL | N/A | Vector Laboratories | FL-1081-1 |
| *Sambucus nigra* lectin (SNA)—CY3 | Sialic acid linked to N-acetylgalactosamine and galactose | 4J–4L | 100 µg/mL | N/A | Vector Laboratories | CL-1303-1 |
| *Limax flavus* lectin (LFA)—FITC | Sialic acid | 5A–5C | 100 µg/mL | N/A | EY Laboratories | F-5101-1 |
| Wheat germ agglutinin (WGA)—Alexa Fluor 594 | *N*-Acetylglucosamine, *N*-acetylneuraminic acid (sialic acid) | 5D–5F | 50 µg/mL | N/A | Thermo Fisher Scientific | Invitrogen W11262 |
| Succinylated wheat germ agglutinin (sWGA)—FITC | N-Acetylglucosamine | 5G–5I | 100 µg/mL | N/A | Vector Laboratories | FL-1021S-5 |
| Peanut agglutinin (PNA)—Alexa Fluor 594 | Terminal $\beta$-galactose | 5J–5L | 50 µg/mL | N/A | Thermo Fisher Scientific | Invitrogen L32459 |
| Alizarin Red S | Calcium | 6A–6C | 1 mg/mL | N/A | Millipore Sigma | Sigma-Aldrich A5533 |

Species reactivity values are reported based on the manufacturers' and published literature. Lectins and dyes do not have specific species reactivities and are labeled as N/A. B, bovine; H, human; M, mouse; P, pig; R, rat.

accumulation or decreasing the load of high-risk drusen in AMD.

## Materials and Methods

### Primary Porcine RPE Isolation and Culture

Primary porcine RPE isolation and culture were performed according to our previously published protocol.[34] In brief, fresh porcine eyes (<6 hours postmortem) were obtained from a local abattoir and were transported on wet ice (~4°C) for immediate dissection. Following thorough disinfected by immersion in povidone iodine prep solution, the RPE was exposed via mechanical removal of the cornea, lens, vitreous body, and retina. The primary RPE was isolated from the remaining globe via enzymatic dissociation using two 30-minute incubations in freshly prepared 0.25% trypsin in L-15 media at 37°C. Dissociated RPE cells were recovered, incubated for 2 minutes in 1% DNase I, and purified via centrifugation on a 40% Percoll cushion with 0.01-M $Na_2PO_4$ and 0.15-M NaCl (pH 7.4). Isolated and purified RPE was resuspended in Dulbecco's Modified Eagle Medium, high-glucose, HEPES cell culture medium with 10% fetal bovine serum and 1% antibiotic–antimycotic and plated on the upper chambers of 24-well polyethylene terephthalate (PET) Transwell membranes at a concentration of 25,000 cells per well (100,000 cells/mL media). At this seeding density, RPE cells do not proliferate but form a monolayer with continuous cobblestone morphology and dense pigmentation while also expressing markers of tight junction integrity (e.g., Zo-1) and RPE identity (e.g., Mitf) that can be maintained without passaging in a 5% $CO_2$ and 37°C incubator with full media changes performed every 3 to 5 days (Supplementary Figs. S1A–S1C). Three separate isolations of primary porcine RPE were performed and utilized throughout the study.

Investigative Ophthalmology & Visual Science

### Tissue Fixation, Preparation, and Cryosectioning

At 20 weeks after isolation, RPE cultures were washed once in PBS and fixed for histological analysis in 4% paraformaldehyde in 0.1-M Sorensen's phosphate buffer for 30 minutes at room temperature. Transwell membranes were cryoprotected via sucrose series (30 minutes in 10% sucrose, 30 minutes in 20% sucrose, and overnight in 30% sucrose) and cryosectioned at 6-µm thickness according to previously published protocols.[49]

Human donor globes recovered from a non-transplant 81-year-old donor (VisionGift, Portland, OR, USA) with confirmed diagnosis of bilateral dry AMD were delivered fresh on wet ice within 24 hours postmortem and immediately prepared for fixation. The anterior chamber, iris, lens, and vitreous were removed mechanically, and the remaining posterior poles were fixed in 4% paraformaldehyde in 0.1-M Sorensen's phosphate buffer overnight at 4°C. Eyes were cryoprotected via sucrose series (10%, 20%, and 30% sucrose overnight at 4°C) and sectioned sagitally at 14-µm thickness onto glass microscope slides (Fisherbrand Superfrost Plus; Fisher Scientific, Waltham, MA, USA). On histological sections, the drusen location was defined by the proximity of each deposit to the fovea, with drusen located within a 6 mm diameter area centered on the fovea being defined as "central" (which contains the macula), and drusen located between 6 mm of the fovea extending laterally to the ora serrata defined as "peripheral."[50] All experiments conformed to all relevant regulations governing the use of animal and human tissues in research and were performed in accordance with the ARVO Statement for the Use of Animals in Ophthalmic and Vision Research and with an exemption for the use of postmortem human tissue from the Institutional Review Board of the Medical College of Wisconsin.

### Immunofluorescence and Lectin Histochemistry

Antibody staining procedures of cryosectioned RPE and human donor tissue were carried out according to previously published protocols (Table 1).[49] Secondary antibody controls are presented for all antibodies in Supplementary Figure S3. Lectin staining was performed based on previously published lectin staining of human drusen.[51] Briefly, cryosections were rehydrated with PBS for 30 minutes and blocked for 15 minutes with 1 mg/mL BSA in PBS. Sections were washed twice with PBS for 10 minutes and incubated for 30 minutes at room temperature with the appropriate lectin in PBS containing 1 mg/mL BSA (Table 1). Slides were washed three times for 10 minutes each with PBS, counterstained with Hoechst, and washed three more times with PBS before being mounted. Staining was imaged using a confocal microscope and imaging software (Nikon Eclipse 80i and NIS-Elements; Nikon, Tokyo, Japan). In some cases, exposure was modified slightly for primary RPE imaging versus human tissue imaging for image clarity. *Z*-stacks were compressed using ImageJ/Fiji image processing software (National Institutes of Health, Bethesda, MD). Unstained control sections can be found in Supplementary Figures S3 to S4.

### MALDI-IMS and Optical Imaging

Autofluorescence images were taken of the section prior to matrix application using the standard 4′,6-diamidino-2-phenylindole (DAPI), enhanced green fluorescent protein, and DSRed fluorescent filters and brightfield in a ZEISS Axioscan Z1 slide scanner (Carl Zeiss Microscopy, Oberkochen, Germany). The matrices, 2,5-dihydroxyacetophenone (DHA) and 1,5-diaminonaphalene (DAN), were applied using a custom in-house-designed sublimation device for positive and negative ion mode analysis, respectively. Data were acquired on a timsTOF fleX instrument (Bruker Daltonics, Bremen, Germany) with methods optimized for a 5-µm pixel size.[52] Data were acquired over a mass/charge ratio ($m/z$) of 500 to 2000 with 80 shots per pixel in regions identified as containing RPE cells using the pre-autofluorescence images. MALDI-IMS images were generated using SCiLS software (Bruker Daltonics), and the brightfield and autofluorescence images were processed using QuPath (https://qupath.github.io/). All MALDI-IMS experiments were performed untargeted, and molecular identifications were based on exact mass with a mass error of 2.26 to 5.60 ppm. All data have been deposited to Zenodo and are publicly accessible.

## Results

### Localization of Complement Cascade Protein Components in Porcine Ex Vivo Sub-RPE Deposits and Human Drusen

Dysregulation of the complement cascade has been demonstrated to play a critical role in the physiopathology of AMD. Several known alleles, including complement factor H (e.g., Y402H), confer a significantly higher (>sevenfold) risk of disease progression through a variety of different mechanisms, including recruitment of immune cells to the choroidal space, promotion of chronic ocular inflammation, and increased oxidative stress.[53,54] As a consequence of their prominence in AMD pathology and the widespread interest in exploring whether inhibitors of various complement components may have therapeutic benefits in preventing disease progression, we first characterized the tissue localization of complement component 9 (C9), complement factor I (CFI), and CFH. We compared three independent preparations of 20-week-old primary RPE monolayer cultures (i.e., derived from separate batches of porcine eyes at different time points) to two globes from one human donor with a history of bilateral early dry AMD. Similar to previous reports that have found complement proteins to be relatively abundant within human drusen, C9 was observed to be present within deposits at all globe eccentricities; small (<10 µm) punctate basal linear deposits (BLinDs) were mainly observed in the region of the macula (Fig. 1A) and larger (>30 µm) C9-filled drusen were present more peripherally (Fig. 1B).[17] Primary RPE grown as a monolayer on PET membranes does not exhibit any obvious regional differences, as both small and large sub-RPE deposits were distributed relatively evenly across the membrane at 20 weeks.[55] Deposits typically accumulated between the basal lamina of the RPE monolayer and the upper aspect of the Transwell membrane, which in our culture system is mechanically analogous to BrM in that it provides a rigid, semipermeable barrier on which the RPE monolayers are supported and across which nutrients and oxygen can pass (Supplementary Fig. S2). C9 was similarly localized throughout both small and large sub-RPE deposits in all three independent monolayer preparations, suggesting that this common component of both macular and peripheral human drusen (Figs. 1A, 1B) is also common in spontaneous sub-RPE deposits (Fig. 1C, white arrows).

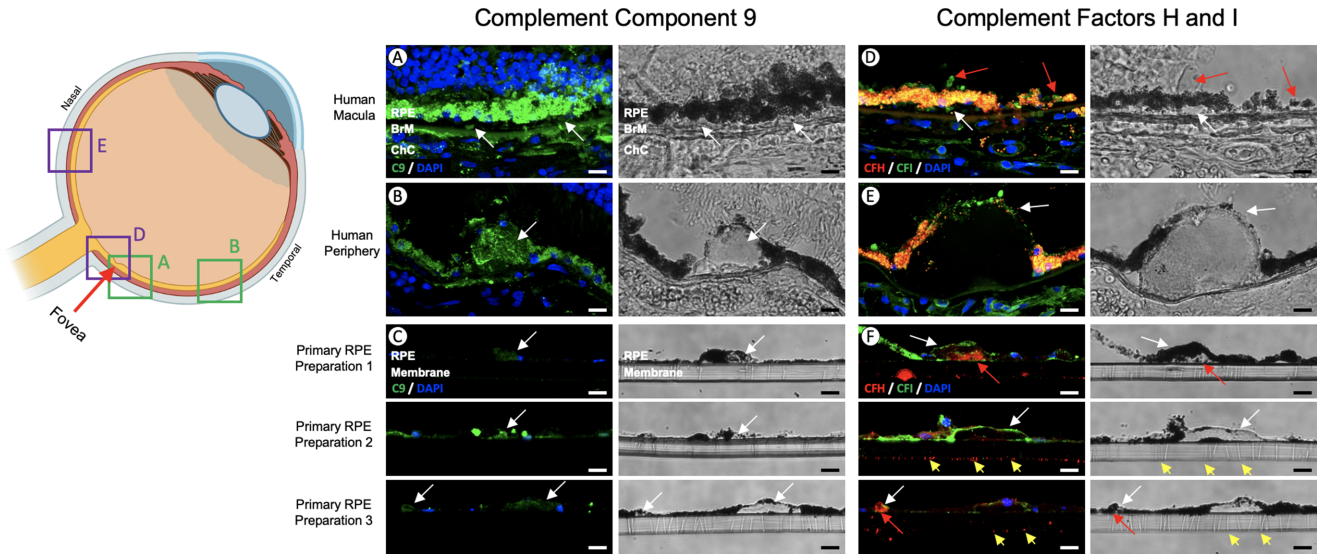


**Figure 1.** Complement protein expression in sub-RPE deposits. (**A–F**) Primary porcine RPE cultured on Transwell membranes and human tissue was probed for C9 (**A–C**, *white arrows*), CFH (**D–F**, *red* and *yellow arrows*), and CFI (**D–F**, *green* and *white arrows*); corresponding brightfield images are shown. All tissues were counterstained with Hoechst to visualize nuclei. *Scale bars*: ~10 µm.

CFI was also present in both macular and peripheral human tissues, but with strikingly different localization. CFI expression was punctate and restricted to BLinDs (Figs. 1D, 1E, white arrow) and sub-retinal drusenoid deposits (also known as reticular pseudodrusen) (Fig. 1D, red arrow) within the macular region but was distributed more widely across the apex of large peripheral drusen, frequently in areas of extensive RPE atrophy (Fig. 1E, white arrow). We observed that this latter expression pattern was closely recapitulated in all three preparations of primary porcine RPE monolayer, with CFI localized to a thin layer overlaying the sub-RPE deposits (Fig. 1F, white arrows), indicating that in this respect cultured sub-RPE may exhibit a more peripheral drusen phenotype.

CFH staining was observed to be indistinguishable from background autofluorescence in human donor globes at both macular and peripheral eccentricities, indicating that the protein is either largely absent or present at low levels within this specimen, as has been observed previously in other histological studies of donor globes with early AMD.[56] CFH-positive puncta were observed sporadically across membranes from all three primary RPE preparations, being observed in some deposits but not in others even within the same histological section (Fig. 1F, red arrows). Interestingly, punctate CFH staining was also observed at the bottom aspect of the PET membrane and especially in areas with visible pores (Fig. 1F, yellow arrows), indicating that CFH may be being secreted basally from the RPE monolayers.

## Apolipoproteins Have Comparable Localization Patterns in Primary Human Drusen as in Monolayers of Cultured Porcine RPE

Various apolipoproteins and lipid species are thought to be critical for the onset and progression of AMD. It has been proposed that age-related alterations (e.g., thickening, stiffening) of BrM and the choriocapillaris impair the transport and clearance of lipids and their carriers into the plasma, leading to the abnormal retention of cholesterol-rich apolipoprotein containing particles within the RPE, catalyzing the subsequent formation of BlinDs and drusen.[17,57,58] As a consequence, both the presence and localization of apolipoproteins (specifically, ApoE and ApoJ) in "drusen-in-a-dish" model systems relative to their distribution in human donor tissue are of importance to the utility of a model for screening therapeutics aimed at altering lipid export, such as ApoA to ApoI mimetic peptides.[59] As expected, drusen located within both the macular and peripheral regions of human donor eyes were found to be positive for the presence of lipid carriers ApoE and ApoJ. Staining was observed to be more intense and uniformly distributed in larger peripheral drusen than in macular drusen and BLinDs, where the signal was more punctate (Figs. 2A, 2B, 2D, 2E, white arrows). Encouragingly, across all three independently cultured preparations of RPE monolayers, we routinely observed ApoE and ApoJ immunofluorescence signals distributed evenly throughout and restricted to the sub-RPE deposits (Figs. 2C, 2F, white arrows), indicating that these proteins may be equally important for formation and growth of "drusen" in a cell culture environment as in situ in AMD.

## Abnormal Deposition of Extracellular Matrix Proteins Occurs Consistently in Cultured Sub-RPE Deposits Compared to Primary Human Macular and Peripheral Drusen

Twenty-week-old RPE monolayers and human AMD globes were also probed for the presence of several extracellular matrix proteins that are critical in maintaining homeostasis of the RPE basal lamina and BrM.[17] Vitronectin, which participates in photoreceptor outer segment phagocytosis and RPE attachment to BrM, was observed throughout the RPE, BrM, and choroid within the macula, but it was largely absent from the drusen themselves (Fig. 3A, white arrow). By contrast, at more peripheral locations, vitronectin protein was distributed prominently throughout large drusen with relatively lower intensity staining observed in neighboring tissues, such as the RPE (Fig. 3B,

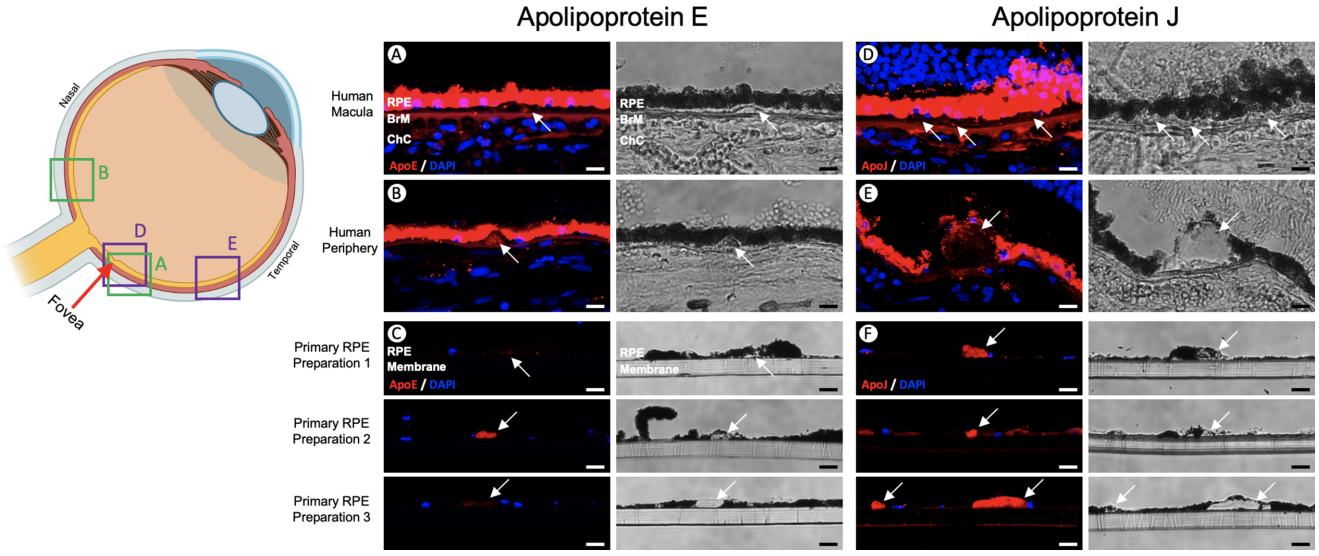


**Figure 2.** Apolipoprotein expression in sub-RPE deposits. (**A–F**) Primary porcine RPE cultured on Transwell membranes and human tissue was probed for ApoE (**A–C**, *white arrows*) and ApoJ (**D–F**, *white arrows*); corresponding brightfield images are shown. All tissues were counterstained with Hoechst to visualize nuclei. *Scale bars*: ~10 µm.

white arrow). In cultured RPE from all three preparations, vitronectin was present prominently throughout the Transwell membrane, indicating that the protein was secreted basally from the polarized monolayers. Interestingly, sub-RPE deposits in cultured monolayers were observed that recapitulated either a macular or peripheral drusen phenotype, with examples of deposits in which vitronectin was located only on the deposit margins (Fig. 3C, white arrows), was distributed evenly throughout the deposit (Fig. 3C, red arrowheads), or was absent from the deposits altogether (Fig. 3C, yellow arrow), indicating a high degree of heterogeneity.

Collagen VI aggregates have been implicated in AMD pathology and were observed to be present within the basal aspects of both human macular and peripheral drusen (Figs. 3D, 3E, white arrows), whereas in primary RPE cultures collagen VI was distributed evenly throughout the cellular monolayer (Fig. 3F, white arrows), was secreted basally through the membrane (yellow arrows), and was concentrated in many sub-RPE deposits (red arrows), compared to secondary-only staining controls (Supplementary Fig. 3).[60]

Sub-RPE deposits grown in cultured monolayers also demonstrated clear aggregation of both collagen types IV and V that were consistent across all three independent preparations of primary porcine RPE (Figs. 3I–L, white arrows). This is in contrast to the human tissue sections, where collagen types IV and V appear to be absent from both macular and peripheral human drusen (Figs. 3G, 3H, 3J, 3K, red arrows) and the epithelial basal laminar.

## Lectin Staining Reveals Widespread Accumulation of Glycans in Human Macular and Peripheral Drusen That are Recapitulated by Porcine Sub-RPE Deposits

As glycans and glycoproteins have been shown to accumulate in drusen recovered from human donor tissue, herein we employed a panel of lectins and agglutinins to probe for the presence of polysaccharide and carbohydrate species within 20-week aged sub-RPE deposits compared to drusen of human dry AMD donor globes.[51,61] The lectins included in our panel were selected based on having known binding targets and the likelihood that glycoproteins containing such moieties may reasonably be expected to accumulate in either human drusen or sub-RPE deposits. *Sambucus nigra* agglutinin (SNA) (Figs. 4A–C) and *Limax flavus* agglutinin (LFA) (Figs. 4D–F) were chosen specifically because they preferentially bind glycoconjugates containing sialic acid or other sialylated glycans, which are known to be present throughout the inter-photoreceptor matrix. Similarly, *Ricinus communis* agglutinin I (RCA I) (Figs. 4G–I) and peanut agglutinin (PNA) (Figs. 4J–L) bind galactose–galactosamine disaccharides or terminal *N*-acetylgalactosamine residues, which are enriched in the rod and cone inner/outer segments.[62,63] SNA lectin was observed to strongly (Figs. 4A, 4B, white arrows) and specifically (Supplementary Fig. S4) stain the majority of drusen observed at both macular and peripheral eccentricates in human AMD globes. It was also uniformly present throughout sub-RPE deposits across all three independent porcine RPE isolations (Fig. 4C, yellow arrows), indicating that sialylated glycans are a key drusen component and are accurately recapitulated by our model porcine RPE system. Interestingly, within individual histological sections, we observed that some large peripheral drusen were negative for SNA (Fig. 4B, green arrows), suggesting that accumulation of sialylated glycans may occur preferentially in certain drusen subtypes (e.g., soft versus hard).

LFA lectin similarly stained both human drusen and porcine sub-RPE deposits, although staining intensity was lower and the distribution more heterogeneous, especially in large peripheral drusen (Figs. 4D–F, white arrows), indicating an asymmetric deposition of glycoconjugates containing terminal $\alpha$2,6-linked sialic acid residues.

RCA I–positive material was observed in drusen at peripheral locations (Fig. 4G, white arrows) but not macular (Fig. 4H, red arrows), indicating a differential accumulation of

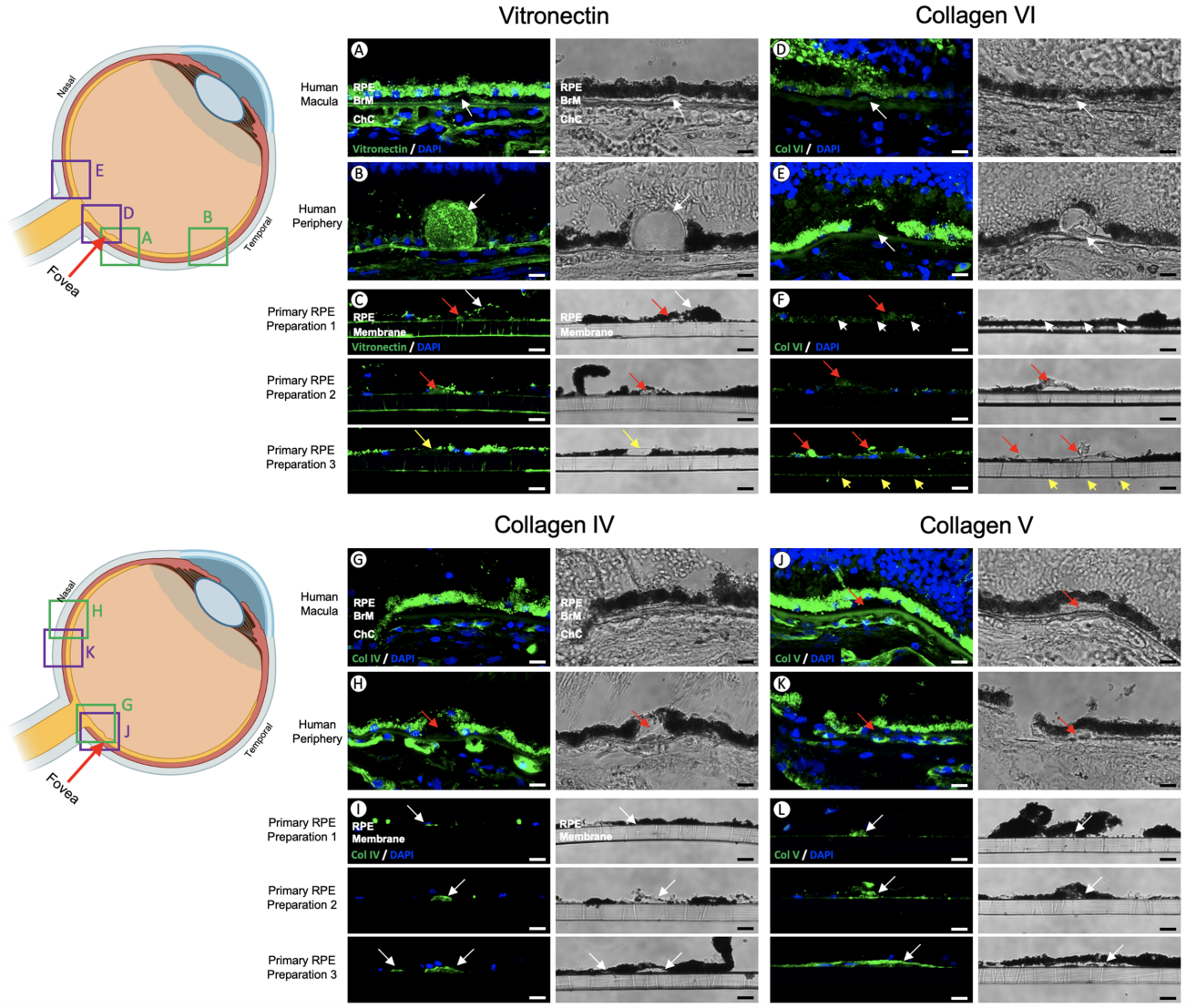


**Figure 3.** Extracellular matrix protein expression in sub-RPE deposits. (**A–L**) Primary porcine RPE cultured on Transwell membranes and human tissue was probed for a variety of extracellular matrix and basement membrane proteins including vitronectin (**A–C**), collagen VI (**D–F**), collagen IV (**G–I**), and collagen V (**J–L**); corresponding brightfield images are shown. The *white arrowheads* indicate areas of increased vitronectin expression. The *yellow arrows* indicate areas of decreased vitronectin expression. The *white arrows* indicate regions of protein accumulation or aggregation. All tissues were counterstained with Hoechst to visualize nuclei. *Scale bars*: ~10 µm.

*β*-linked terminal D-galactose containing moieties across the retina. Sub-RPE deposits crossed all three independent preparations of porcine RPE and were observed to uniformly and strongly stain with RCA I (Fig. 4I, white arrows), indicating that lab grown sub-RPE deposits may more closely mimic peripheral than macular drusen. By contrast, PNA lectin, which binds terminal D-galactose residues known to preferentially localize to the extracellular matrix surrounding cone photoreceptors, was observed to be effectively absent in all drusen observed in human donor globes regardless of location (Figs. 4J, 4K, yellow arrows) but was widespread throughout porcine sub-RPE deposits, despite the absence of any photoreceptor contribution (Fig. 4L, white arrows).[64]

We additionally stained using lectins that bind various oligomannose-type and hybrid- and biantennary-complex–type *N*-glycans (concanavalin A [ConA]) or glycoconjugates that prominently feature *N*-acetylglucosamine (*Lens culinaris* agglutinin [LCA] and succinylated wheat germ agglutinin [sWGA]) or branched poly-*N*-acetyllactosamine residues (WGA), which have been described previously to be present in drusen from human AMD donors but the cellular/tissue origins of which remain uncertain.[51] ConA-positive (Figs. 5A–C, white arrows) and LCA-positive (Figs. 5D–F, white arrows) material was observed in both small macular and large peripheral drusen and was observed uniformly across sub-RPE deposits from all three preparations, indicating that accumulation of oligomannose-rich and fucosylated *N*-glycans may be a uniform feature of drusen regardless of type and is accurately recapitulated in sub-RPE deposits. By contrast, WGA- and sWGA-positive material was largely absent from macular drusen but was observed extensively throughout peripheral drusen, albeit with differential expression patterns, wherein WGA staining was largely uniform and sWGA staining was punctate throughout large peripheral basal laminar deposits (Figs. 5G–L, white arrows). This finding indicates that accumulation of glucosamine-

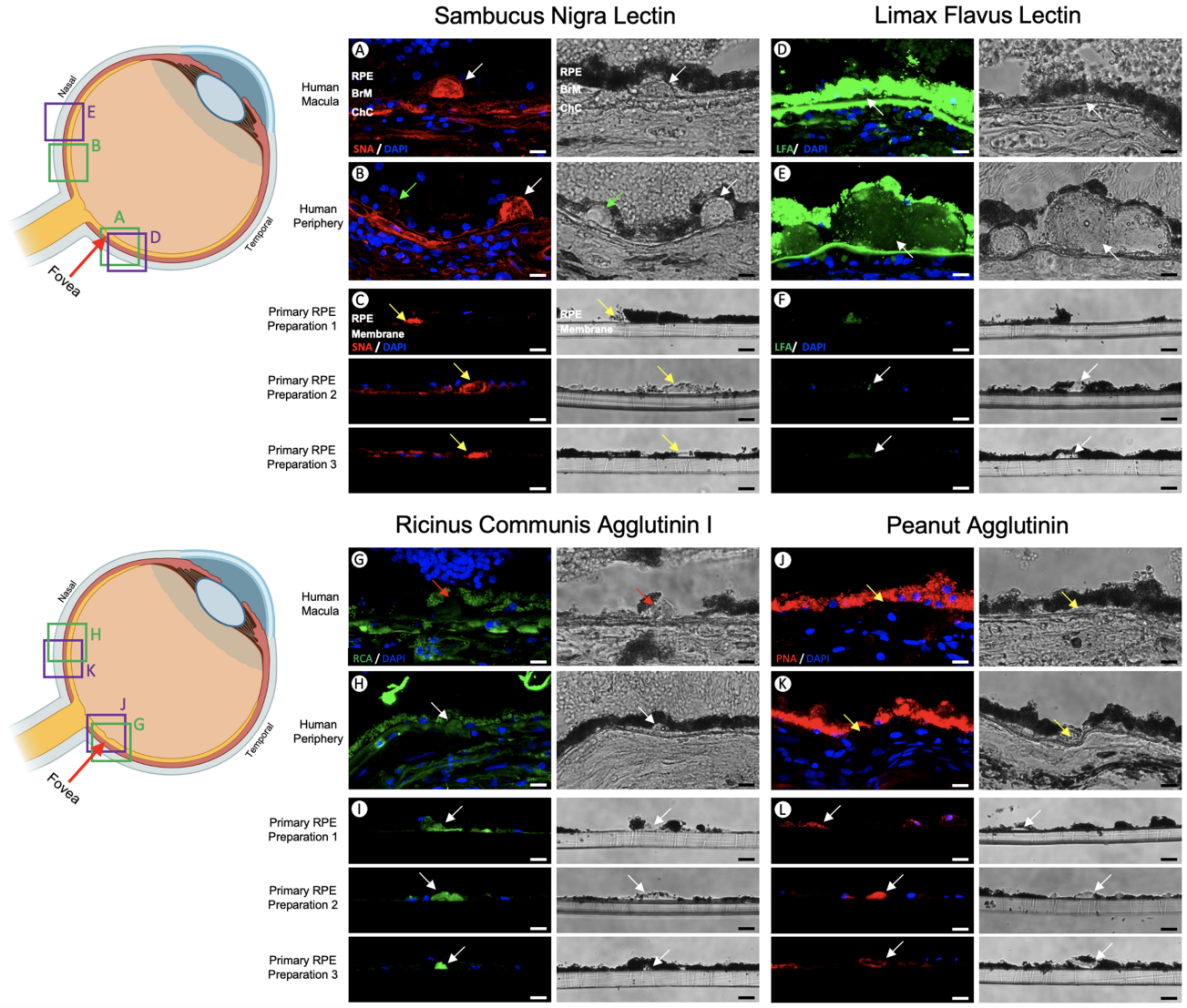


**Figure 4.** Lectin staining of sub-RPE deposits and human drusen. (**A–L**) Primary porcine RPE cultured on Transwell membranes and human tissue was probed with a variety of lectins and agglutinins, including SNA (**A–C**), LFA (**D–F**), RCA I (**G–I**), and PNA (**J–L**); corresponding brightfield images are shown. *White arrows* indicate regions of lectin binding. The *white arrowheads* indicate drusen with decreased SNA binding. All tissues were counterstained with Hoechst to visualize nuclei. *Scale bars*: ~10 µm.

and lactosamine-containing glycoconjugates may be more a feature of peripheral (likely hard) drusen and also occurs in porcine monolayers, where WGA- and sWGA-positive material was routinely observed across all preparations (Figs. 5I, 5L).

## Sub-RPE Deposits in Ex Vivo Monolayers Demonstrate Limited Calcification

Alizarin Red was used to probe for the presence of calcium mineralization within sub-RPE deposits and drusen, a hallmark of end-stage AMD wherein calcified drusen are frequently associated with areas of degenerating RPE.[48,65] Interestingly, in the context of previous reports that have demonstrated the presence of calcium-containing species, such as hydroxyapatite, throughout human drusen, Alizarin Red staining did not reveal any obvious positive material in the macular region of the donor globes (Fig. 6A), although some signal was observed in human peripheral drusen (Fig. 6B, white arrow). Similarly, although some areas of calcium deposition were present in porcine sub-RPE deposits, these were sporadic and uncommon, indicating that 20 weeks of culture may not be sufficient for mineralization to occur (Fig. 6C, white arrows).

## Lipid Accumulation in Sub-RPE Deposits and Pores of the Transwell Membrane in RPE Monolayers More Closely Resembles Human Macular Drusen

To probe for the presence of polar and neutral lipid species, such as esterified cholesterol, sections were stained with Nile red, a vital dye that fluoresces yellow to deep red in the presence of various lipid species. In sections of human AMD globes from the macula, diffuse Nile red staining was evident throughout BrM (Fig. 7A, green arrows), and more punc-

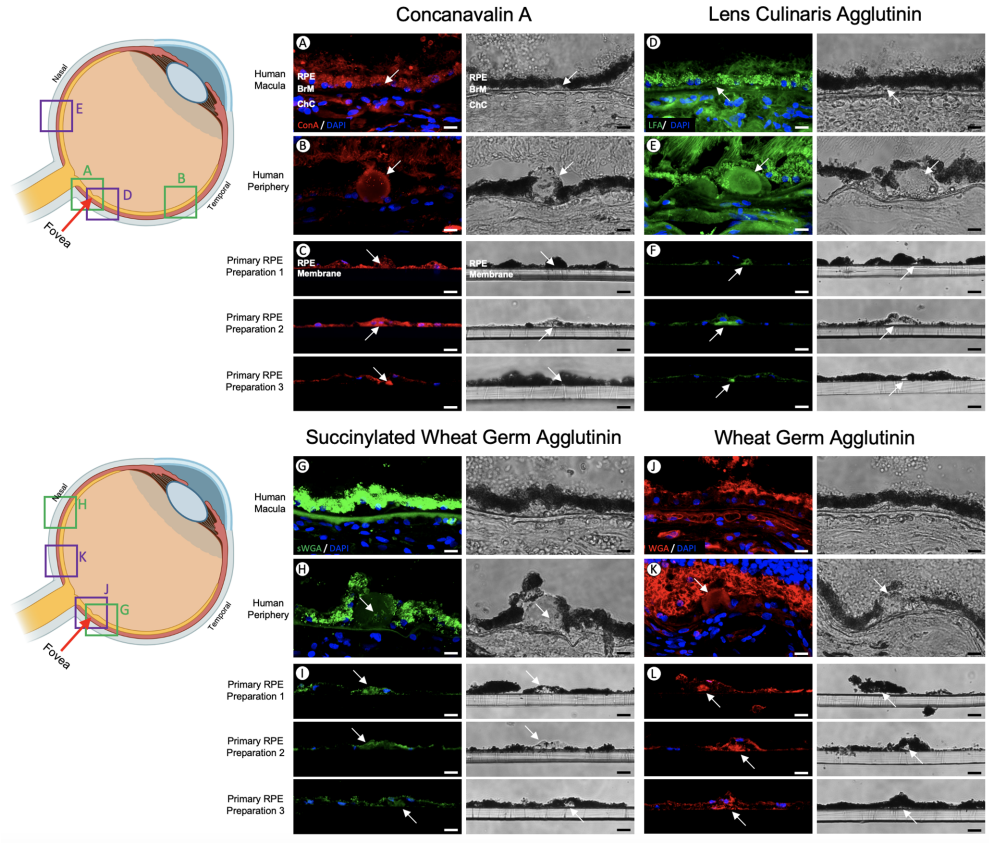


**Figure 5.** Lectin staining of sub-RPE deposits and human drusen. (**A–L**) Primary porcine RPE cultured on Transwell membranes and human tissue were probed with a variety of lectins and agglutinins including ConA (**A–C**), LCA (**D–F**), sWGA (**G–I**), and WGA (**J–L**); corresponding brightfield images are shown. *White arrows* indicate regions of lectin binding. All tissues were counterstained with Hoechst to visualize nuclei. *Scale bars*: ~10 µm.

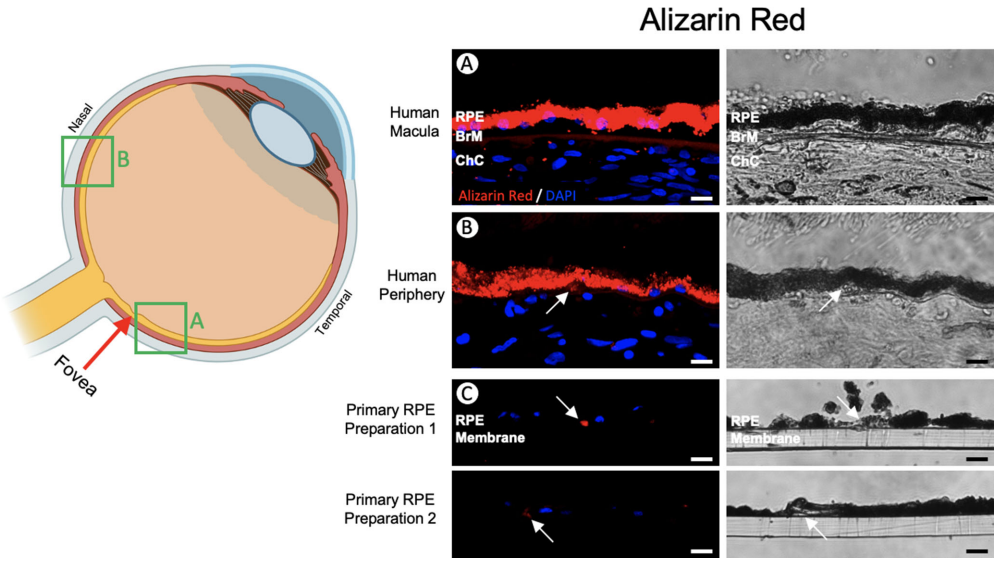


**Figure 6.** Calcium deposits in sub-RPE deposits and human drusen. (**A–C**) Human tissue from macula lutea (**A**) and periphery (**B**) and primary porcine RPE cultured on Transwell membranes (**C**) were probed for calcium deposits using Alizarin Red stain and are shown with corresponding brightfield images. The *white arrows* indicate regions of positive Alizarin Red staining. All tissues were counterstained with Hoechst to visualize nuclei. *Scale bars*: ~10 µm.

Investigative Ophthalmology & Visual Science

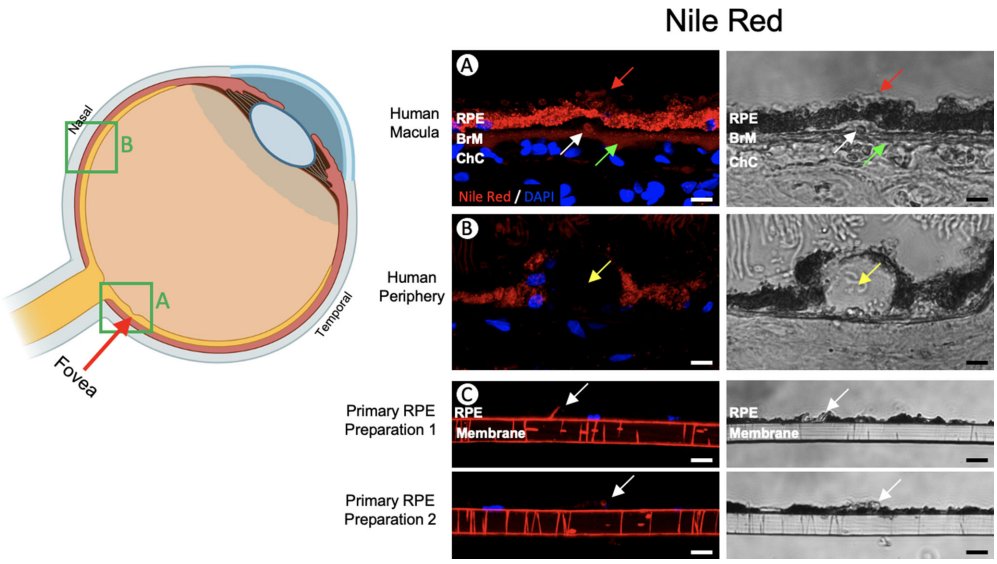


**Figure 7.** Lipid deposition in sub-RPE deposits and human drusen. (**A–C**) Human tissue from macula lutea (**A**) and periphery (**B**) and primary porcine RPE cultured on Transwell membranes (**C**) were probed for lipids using Nile red stain and are shown with corresponding brightfield images. The *white arrows* indicate regions of positive Nile red staining. The *arrowheads* indicate enriched lipid staining in BrM. All tissues were counterstained with Hoechst to visualize nuclei. *Scale bars*: ~10 µm.

tate lipid accumulation was also evident in BLinDs (Fig. 7A, white arrow) and sub-retinal drusenoid deposits (Fig. 7A, red arrow). A similar staining pattern was observed in 20-week-old cultures of primary porcine RPE, wherein punctate Nile red staining was evident within and on the margins of the sub-RPE deposits (Fig. 7C, white arrows). Interestingly, there was also diffuse staining throughout the pores of the Transwell membrane, strongly suggesting that RPE monolayers basally secrete lipid species. In contrast, Nile red staining appeared to be absent from human drusen observed at peripheral eccentricities (Fig. 7, yellow arrows) and did not exceed background autofluorescence levels throughout the RPE and BrM (Supplementary Fig. S4). This finding indicates that lipid deposition is more a feature of soft macular than hard peripheral drusen and that in this important respect "drusen in a dish" may be more representative of pathogenic deposits associated with increased risk of AMD progression.[66–68]

## IMS Reveals Accumulation of Multiple Very-Long-Chain Ceramide Species at the Margins of Sub-RPE Deposits

Building upon evidence of lipid deposition provided by our Nile red staining, we performed IMS in order to accurately identify the various lipid species that accumulate in sub-RPE deposits (Fig. 8). The signal at *m/z* 549.1067 was detected

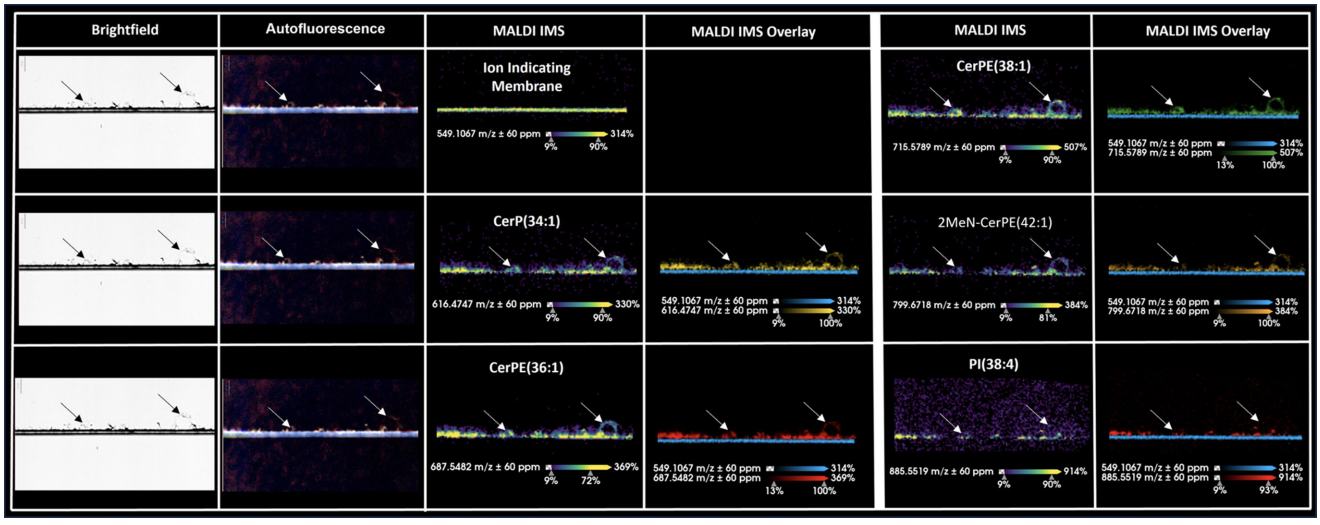


**Figure 8.** IMS analysis of lipid localization in sub-RPE deposits. Brightfield (*column 1*), autofluorescence (*column 2*), and MALDI-IMS (*columns 3–6*) images of sub-RPE deposits on Transwell membranes. *Arrows* indicate the locations of deposits. IMS images show signals specific for the membrane (*m/z* 549.1067) and lipids surrounding deposits (*m/z* 616.4747, *m/z* 687.5482, *m/z* 715.5789, *m/z* 799.6718, and *m/z* 885.5519). IMS overlays show RPE and deposit signal locations relative to the membrane, visualized using a heatmap with a mass window of 60 ppm. Identifications were based on accurate mass assignments (mass error = 2.26–5.60 ppm) to lipids in the LIPID MAPS database, and all ceramide lipids have been reported in neural retina, RPE, and choroid, as well as in drusen and basal laminar deposits.[70,97]

Investigative Ophthalmology & Visual Science

**Table 2.** Lipid Species Detected by IMS and Reference Locations

| Lipid | Measured Mass (*m/z*) | Theoretical Mass (*m/z*) | Mass Error (ppm) | Human Retina Mass (*m/z*)* | Human Retina Location* | Seen in Human Deposits? |
|---|---|---|---|---|---|---|
| CerP 34:1 | 616.4747 | 616.4712 | 5.68 | 616.471 | RPE, choroid | Yes† |
| CerPE 36:1 | 687.5482 | 687.5447 | 5.09 | 687.543 | RPE, choroid | Yes† |
| CerPE 38:1 | 715.5789 | 715.5760 | 4.05 | 715.576 | RPE, HFL, INL | Yes† |
| 2MeN–CerPE 42:1 | 799.6718 | 799.6694 | 3.00 | 799.667 | RPE | Yes‡ |
| PI 38:4 | 885.5519 | 885.5499 | 2.26 | 885.549 | RPE, HFL, ONL, GCL | No |

Summary table describes the lipid species and actual mass measured via IMS in sub-RPE deposits in porcine RPE monolayers with reference to theoretical mass based on a given error. Also listed are previously reported locations of these species in human drusen based on the cited works. GCL, ganglion cell layer; HFL, Henle fiber layer; INL, inner nuclear layer; ONL, outer nuclear layer.

in the region of the membrane and served as a guide in the IMS overlay images to visually observe signals above the membrane due to deposit formation. The ceramides (Fig. 8, Table 2) included ceramide–phosphate (CerP 34:1 at *m/z* 616.4747) and ceramide–phosphatidylethanolamines (CerPE 36:1 and CerPE 38:1 at *m/z* 687.5482 and *m/z* 715.5789, respectively). Two additional signals were detected at *m/z* 799.6718 and *m/z* 885.5519, corresponding to 2MeN–CerPE (42:1) and PI (38:4), respectively; however, the former signal is likely due to fragmentation of sphingomyelin (42:1) during the MALDI process.[69] In line with the Nile red staining and our previously published RPE culture protocol, detectable signals corresponding to the accumulation of lipid species (i.e., ceramides) appeared only at the margins of the sub-RPE deposits, with no signals detectable within the deposits themselves. Although we were unable to perform IMS directly on the human donor globes due to differences in fixation protocols, with the exception of PI 38:4, all of these ceramide species have previously been reported to be present in ocular tissues, including the neural retina, RPE, and choroid (summarized in Table 2) and have been observed in human drusen and basal laminar deposits.[70]

## Discussion

Due to its complex nature, wherein disease onset and progression are impacted by multiple environmental and genetic risk factors, the dry form of AMD has proven particularly difficult to accurately model in a research environment. Although several animal models have been developed that recapitulate certain aspects of AMD pathology, including sub-RPE basal linear/laminar deposits, complement dysregulation, hypo-/hyperpigmentation, photoreceptor/RPE atrophy, and inflammation, no model fully encompasses all aspects of AMD disease progression.[4,19–22,25] A problem facing the development of novel therapeutics targeting pathogenic accumulation of drusen within the central retina, such as gene or cell therapies aimed at reducing druse volume, is that rodent models—which are most commonly utilized due to their small size, low maintenance costs, and ease of genetic manipulation—are anatomically dissimilar from humans. Specifically, they do not possess a fovea, and the rod-dominant mouse/rat retina more closely resembles the human near-periphery in terms of rod-to-cone ratio (30:1).[25,50,71] Furthermore, the accumulation of basal linear/laminar deposits in transgenic animal models, such as complement knockout (e.g., $Cfh^{-/-}$) or chemokine knockout ($Ccr12^{-/-}$ or $Cx3cr1^{-/-}$) mice or wild-type aged animals, including NHPs, takes years (>12–16 months) or decades (>15 years) to occur, effectively limiting their utility for even low-throughput screening of new therapeutic approaches.[25,72–74]

As a consequence of these limitations, our research group and others have focused on the development of cell culture models of dry AMD, which if properly characterized may offer a cost-scalable and manipulatable model system that can be used for high-throughput screening of novel AMD therapeutics before progression to preclinical animal studies. These systems typically consist of RPE cell monolayers grown on a porous support, such as a PET membrane, and are cultured with or without additives (e.g., rod outer segments, nicotinamide) over a period of several weeks. The majority of studies have been performed using ARPE-19 cells, a spontaneously arising immortalized line, which have been used to study epithelial–mesenchymal transition, complement activation, phagocytosis defect, and inflammatory processes, all of which have been implicated in AMD disease progression.[34,75–81] However, in recent years, it has been recognized that there are numerous disadvantages to the use of this cell line, including an abnormal karyotype, poor phenotypic fidelity, and an altered transcriptomic/proteomic profile that differentiate it from human primary RPE cells.[34,82,83]

As a consequence, our group and others have focused on the use of either iPSC-derived or primary RPE cells harvested from donor globes. Although ideally such studies would exclusively utilize human primary RPE to maximize clinical relevance, human donor globes are costly, relatively scarce (especially when a confirmed diagnosis of AMD is required), and often not viable for culture due to longer than ideal (>6 hours) postmortem time to recovery.[34–40] We have instead built upon several previous studies by culturing primary RPE from porcine globes—which are inexpensive and readily available from any abattoir—as a model for AMD. Following on from our recently published study that detailed the dynamics of sub-RPE deposit accumulation in porcine RPE monolayers over a period of 6 months using repetitive vital lipid staining and cross-sectional immunohistochemistry to probe for major protein components (e.g., CFH, ApoE, ApoJ), we selected the 20-week time point to perform a more detailed characterization of sub-RPE deposit contents.[55] Specifically, we wished to further describe the protein, lipid, and glycoprotein contents of spontaneously accumulating sub-RPE deposits by combining multiple histopathological approaches with IMS, with a view to determining whether they are truly representative of human primary drusen in dry AMD and whether sub-RPE deposits more accurately recapitulate either macular soft or peripheral hard drusen. Our goal was to better delineate whether such "drusen-in-a-dish"

Investigative Ophthalmology & Visual Science

model systems derived from primary animal tissues could be utilized to screen novel therapies targeting either drusen deposition of clearance, such as ApoE-I mimetic peptides, or complement inhibitors.[48,84,85]

Sub-RPE deposits that spontaneously accumulate in primary porcine monolayer cultures were observed to express numerous known components of primary human drusen, including multiple complement proteins, apolipoproteins, glycans, and extracellular matrix proteins.[17] Importantly, despite being an artificial model system with the only organic components being the RPE cells and the presence of fetal bovine serum in the media, the distribution of several protein/glycan species was remarkably similar between porcine RPE cultured on PET membranes and primary RPE in situ on BrM. For example, vitronectin staining was evident throughout the RPE, drusen, and choroid in human globes and was similarly distributed throughout the sub-RPE deposits and pores of the PET membrane in porcine cultures (Fig. 3), indicating that the model system effectively mimics vitronectin deposition and secretion into drusen and across BrM, which has been implicated in AMD development.[86–88] Similarly, apolipoproteins, which have been reported by numerous groups using histology and mass spectrometry to be highly enriched in human drusen, were observed almost uniformly in both human donor globes at macular and peripheral eccentricities and in sub-RPE deposits across the monolayer.

There were several components, however, such as collagen types IV and V, that showed major differences between cultured sub-RPE deposits and human drusen, such as when both were absent in donor eyes, despite collagen species being reported previously in basal lamina deposits and the epithelial basal laminar.[89] Although collagen IV and VI have been shown to play roles in AMD disease pathology, it is possible that collagen aggregates are not common within human basal laminar or linear deposits, usually remaining within or below BrM, and so were not observed in our specific tissue samples.[60,90–92] In contrast, large aggregations of collagen type IV and V were documented in primary porcine sub-RPE deposits. Although the nature of these deposits is currently unknown, widespread accumulation of various collagen species indicates aberrations in extracellular matrix deposition and trafficking and may potentially be associated with cellular senescence. Alternatively, these deposits may be a byproduct of the highly artificial nature of culturing RPE in monolayers on porous supports, where the composition of the surrounding media (the likely origin of the materials that ultimately accumulate in sub-RPE deposit) differs substantially from the local environment in situ in the eye.

Although utilizing immunohistochemistry, lectins stains, and the lysochrome dye Nile red to characterize the composition of sub-RPE deposits in porcine monolayers versus human donor globes is a relatively low-technology solution that is able to provide only qualitative information as to composition, it has the distinct advantage of being able to preserve spatial information regarding the composition of drusen relative to ocular location or membrane position. This is in contrast to techniques such as traditional bulk mass spectrometry, which can determine the relative compositions of peptides or lipids but typically does so by sampling drusen recovered from multiple regions across multiple donor globes (or membranes). In this manner, we were able to determine, for the first time to the best of our knowledge, that sub-RPE deposits across the membrane are relatively heterogeneous, with some more closely resembling peripheral or macular drusen from humans. One possible explanation for the observed mix of sub-RPE deposit compositions across the culture monolayers may stem from the method by which primary RPE is harvested in bulk from multiple globes before being cultured. Specifically, each of the three independent preparations of RPE monolayers utilized in this study involved the enzymatic isolation and pooling of RPE cells recovered from approximately 50 porcine globes, meaning that each monolayer was a heterogeneous mix of RPE cells taken from across the globe without regard for location and so may exhibit either central or peripheral phenotype when depositing materials that subsequently accumulate into sub-RPE deposits.

As lectin and agglutinin binding has been documented and well characterized in human drusen, this tool was also employed to further characterize the compositional similarities of primary porcine sub-RPE deposits and human drusen.[51,61] In many cases, lectins and agglutinins that have been documented to stain human drusen have also stained porcine sub-RPE deposits with similar binding patterns (LCA, ConA, RCA I, LFA, WGA, and sWGA). However, both SNA and PNA revealed differential patterns of staining, with both being more consistently observed in sub-RPE deposits than in human drusen. This is particularly interesting in the case of PNA lectin, which has been demonstrated not to bind to soft or hard drusen in human eyes but stained positively in primary porcine sub-RPE deposits. That this occurred despite the absence of photoreceptors in our culture system to provide a source of terminal D-galactose residues, which are enriched in the cone outer segment sheath, provides further evidence that drusen accumulation in both human AMD eyes and ex vivo culture models occurs independently and that drusen components are derived only from the RPE and underlying choroidal circulation, rather than containing recycle material from spent outer segment discs. The accumulation of D-galactose containing glycoproteins in sub-RPE deposits, but not in human drusen, does however serve to highlight that ex vivo culture systems, although one of the best tools we have for studying drusen pathobiology in AMD, do not perfectly recapitulate the human disease environment, resulting in distinct compositional differences that must be accounted for when proposing the use of any ex vivo model for screening novel therapeutics.

IMS was employed to investigate in detail the spatial distribution of lipid species within the sub-RPE deposits accumulating under the cultured porcine monolayers, and it clearly showed specific lipids surrounding the deposits above the Transwell membrane. A majority of the observed signals corresponded to ceramides, a class of biologically active lipids known to be involved in cell differentiation and migration inflammation, apoptosis, autophagy, and endoplasmic reticulum stress, among other functions, and which have been observed previously in the human drusen and BLinD (unpublished data courtesy of Kevin Schey, Vanderbilt University).[70,93,94] Furthermore, ceramide dysfunction has been implicated in a number of diseases, including cancer, heart disease, multiple sclerosis, and age-related disease.[93] Interestingly, the species observed in this study are characterized as long-chain ceramides, which, despite being some of the most abundant types of ceramides detected by animal or human cells, have very unclear physiological roles in both normal tissue homeostasis and disease. As such it is not possible to determine the importance of such long-chain ceramides in the formation or maintenance of drusen

**Table 3.** Comparison of Human Drusen and Sub-RPE Deposit Composition

| | Macular Drusen (MD) | Peripheral Drusen (PD) | Sub-RPE Deposits (SRDs) | SRD Resemblance |
|---|---|---|---|---|
| Antibody | | | | |
| C9 | +++ | +++ | +++ | MD and PD |
| CFH | — | — | +, S | None |
| CHI | +++ | +++ | +++ | MD and PD |
| ApoE | ++ | +++ | +++ | PD > MD |
| ApoJ | ++ | +++ | +++ | PD > MD |
| Vitronectin | +, S | +++ | +, S | MD |
| Collagen VI | ++ | ++ | ++, S | MD and PD |
| Collagen IV | | — | +++ | None |
| Collagen V | — | — | +++ | None |
| Lectin | | | | |
| SNA | +++ | ++ | +++ | MD > PD |
| LFL | ++ | + | ++ | MD > PD |
| RCA I | — | ++ | +++ | PD |
| PNA | — | — | +++ | None |
| ConA | +++ | +++ | +++ | MD and PD |
| LCA | + | + | + | MD and PD |
| sWGA | + | ++ | ++ | PD > MD |
| WGA | + | ++ | ++ | PD > MD |
| Dye | | | | |
| Alizarin Red | — | + | + | PD |
| Nile red | ++, S | | ++, S | MD |

Qualitative abundance of each protein or lectin positive materials in human macular drusen, human peripheral drusen, and ex vivo porcine sub-RPE deposits (SRDs). + indicates rare or sporadically observed in MD, PD, or SRDs; ++, commonly observed in majority of MD/PD/SRDs; +++, homogeneously or uniformly expressed in MD, PD, or SRDs; S, likely secreted and observed within BrM (MD or PD) or Transwell membrane (SRDs); –, absent or indistinguishable from background autofluorescence; >, SRDs more closely resemble either MD or PD; none, SRDs do not resemble either MD or PD.

in human eyes with AMD or sub-RPE deposits in our model culture system.[95,96] It should also be noted that, whereas IMS is able to accurately (mass error = 2.26–5.60 ppm) identify individual species of lipids and demonstrate their spatial distribution within the tissue, the technique does not provide information regarding the absolute abundance of each lipid species, which cannot be inferred from signal intensity alone. As such, although our data strongly indicate that long-chain ceramides are present in porcine sub-RPE deposits, further experiments using liquid chromatography–tandem mass spectrometry would be required to quantify the abundance of each species and so determine whether they represent trace elements or major constituents of sub-RPE deposits and human drusen. One intriguing observation from the imaging mass spectrometry data however, is that all the ceramide species appear to surround rather than be located within the sub-RPE deposits. While the reason behind this spatial localization is also unclear, it potentially indicates that ceramides or other sphingolipid species may be forming a membrane or hydrophobic barrier surrounding the inner protein/glycoprotein/mineral-containing core of the deposit.

Based on the totality of the immunohistochemical and IMS data collected as part of this study, it is clear that porcine sub-RPE deposits do not specifically mimic either macular or peripheral drusen but instead express proteins, glycoproteins, and lipid species that are observed in both soft macular and hard peripheral drusen (Table 3). This finding is perhaps unsurprising, because many components are apparently present in both types of drusen, including C9; CFI; collagen *VI*; oligomannose-type, hybrid-type, and biantennary complex–type *N*-glycans (ConA); and *N*-acetylglucosamine glycoconjugates (LCA), so they would also be expected to be present in laboratory-grown sub-RPE deposits. Given that monolayers are created from dissociated suspensions of RPE cells harvested enzymatically from across the globe without regard to eccentricity and are plated together, it is also unsurprising that the composition of sub-RPE deposits across each well is relatively heterogeneous, with some deposits closely resembling lipid-containing soft macular drusen (e.g., Nile red positive) and other semi-calcified hard peripheral drusen (e.g., Alizarin Red positive). As a consequence, if "drusen-in-a-dish" model systems are to be maximally useful for screening therapeutic molecules aimed at altering drusen formation or accumulation, it may be necessary to modify the current culture protocol. Sub-RPE deposits could be forced to more closely resemble the target drusen population—such as by supplementing cultures with lipids to drive formation of more soft macular-reminiscent deposits—or RPE cells could be isolated from specific areas of the globe during enzymatic recovery, such as from underneath the porcine visual streak only.

One obvious limitation of the "drusen-in-a-dish" model as presented here is the time scale (20 weeks) over which monolayers are cultured before being harvested for immunohistochemistry and IMS, which may limit the utility of the model for high-throughput screening of novel therapeutics aimed at modulating drusen contents. The 20-week time point used in this study was selected based on a recently published work by our group that described the kinetics of sub-RPE deposit accumulation over a 24-week time course that revealed deposit number and area peak around 20 weeks.[55] Although it may be possible to select an earlier time point for read-out with the understanding that fewer sub-RPE deposits will be present for analysis, ideally it would beneficial to investigate methodologies to accelerate deposit formation, which may potentially be achieved through manipulation of the culture media to include higher

Investigative Ophthalmology & Visual Science

concentrations of relevant lipid or protein species, for example. However, although these studies would greatly improve the usability of the described "drusen-in-a-dish" system, they fall outside the scope of the current study.

Another limitation of the current study is that we were only able to directly compare the composition of sub-RPE deposits to hard and soft drusen identified in a pair of globes recovered from a single human donor. The small sample size was primarily driven by our desire to compare sub-RPE deposit composition to human drusen from a donor with confirmed dry AMD but without other ocular complications (e.g., choroidal neovascularization, diabetic retinopathy) in order to maximize the likelihood of resolving drusen in situ without confounding tissue damage caused by unrelated pathologies. Although we feel adherence to such strict inclusion criteria was necessary to the goals of this study (where we needed to be able to accurately identify drusen by type and location), it severely limited our donor pool. Nevertheless, given that the majority of druse contents observed in this study have been observed in other published studies assessing the protein, glycoprotein, or lipid contents of human drusen, we do not feel that the small sample size detracts from the overall generalizability of our findings that porcine sub-RPE deposits are compositionally highly similar to primary human drusen.

In conclusion, the authors believe that this study represents the most comprehensive characterization of a "drusen-in-a-dish" model system to date and confirms that sub-RPE deposits grown in a laboratory environment by monolayers of primary RPE cells show a high degree of compositional similarity to macular and peripheral drusen observed in human AMD. Importantly, sub-RPE deposits grown ex vivo occur spontaneously and consistently, potentially allowing these model systems to be used to probe questions relating to the pathobiology of drusen formation or screen the effects of novel therapeutics aimed at modulating drusen accumulation/clearance in a controlled environment and without reliance on scarce human donor tissue. Although accumulation of sub-RPE deposits occurs relatively rapidly (over several weeks) compared with in vivo formation in human AMD patients (where it occurs over decades), future studies may be necessary to try to accelerate the formation of sub-RPE deposit formation through manipulation of the culture system, such as through feeding monolayers with specific protein (e.g., complement components) or lipid (e.g., esterified cholesterol species) components in the media in order to increase the throughput of the model.

## *Acknowledgments*

Supported through generous donations from the Robert A. Brandt Macular Degeneration Fund (DML) and a Research to Prevent Blindness Catalyst Award (KLS). Portions of the figures were created using BioRender.

Disclosure: **E.M. Shaw**, None; **D.M. Anderson**, None; **R. Periasamy**, None; **K.L. Schey**, None; **C.A. Curcio**, Osanni (C), Character BioSciences (C), Ripple (C), Mobius (C); **D.M. Lipinski**, None

## *References*

1. Rein DB, Wittenborn JS, Burke-Conte Z, et al. Prevalence of age-related macular degeneration in the US in 2019. *JAMA Ophthalmol*. 2022;140:1202–1208.
2. Wong WL, Su X, Li X, et al. Global prevalence of age-related macular degeneration and disease burden projection for 2020 and 2040: a systematic review and meta-analysis. *Lancet Glob Health*. 2014;2:e106–e116.
3. Chew EY, Clemons TE, Agron E, et al. Ten-year follow-up of age-related macular degeneration in the age-related eye disease study: AREDS report no. 36. *JAMA Ophthalmol*. 2014;132:272–277.
4. Handa JT, Bowes Rickman C, Dick AD, et al. A systems biology approach towards understanding and treating non-neovascular age-related macular degeneration. *Nat Commun*. 2019;10:3347.
5. Deng Y, Qiao L, Du M, et al. Age-related macular degeneration: epidemiology, genetics, pathophysiology, diagnosis, and targeted therapy. *Genes Dis*. 2022;9:62–79.
6. Lim LS, Mitchell P, Seddon JM, Holz FG, Wong TY. Age-related macular degeneration. *Lancet*. 2012;379:1728–1738.
7. Curcio CA. Antecedents of soft drusen, the specific deposits of age-related macular degeneration, in the biology of human macula. *Invest Ophthalmol Vis Sci*. 2018;59:AMD182–AMD194.
8. Curcio CA. Soft drusen in age-related macular degeneration: biology and targeting via the oil spill strategies. *Invest Ophthalmol Vis Sci*. 2018;59:AMD160–AMD181.
9. Spaide RF, Ho-Spaide WC, Browne RW, Armstrong D. Characterization of peroxidized lipids in Bruch's membrane. *Retina*. 1999;19:141–147.
10. Cankova Z, Huang JD, Kruth HS, Johnson M. Passage of low-density lipoproteins through Bruch's membrane and choroid. *Exp Eye Res*. 2011;93:947–955.
11. Linsenmeier RA, Zhang HF. Retinal oxygen: from animals to humans. *Prog Retin Eye Res*. 2017;58:115–151.
12. Al-Zamil WM, Yassin SA. Recent developments in age-related macular degeneration: a review. *Clin Interv Aging*. 2017;12:1313–1330.
13. Fabre M, Mateo L, Lamaa D, et al. Recent advances in age-related macular degeneration therapies. *Molecules*. 2022;27:5089.
14. Rosenfeld PJ, Brown DM, Heier JS, et al. Ranibizumab for neovascular age-related macular degeneration. *N Engl J Med*. 2006;355:1419–1431.
15. Hadziahmetovic M, Malek G. Age-related macular degeneration revisited: from pathology and cellular stress to potential therapies. *Front Cell Dev Biol*. 2020;8:612812.
16. Age-Related Eye Disease Study Research Group. A randomized, placebo-controlled, clinical trial of high-dose supplementation with vitamins C and E, beta carotene, and zinc for age-related macular degeneration and vision loss: AREDS report no. 8. *Arch Ophthalmol*. 2001;119:1417–1436.
17. Wang L, Clark ME, Crossman DK, et al. Abundant lipid and protein components of drusen. *PLoS One*. 2010;5:e10329.
18. Crabb JW, Miyagi M, Gu X, et al. Drusen proteome analysis: an approach to the etiology of age-related macular degeneration. *Proc Natl Acad Sci USA*. 2002;99:14682–14687.
19. Toomey CB, Kelly U, Saban DR, Bowes Rickman C. Regulation of age-related macular degeneration-like pathology by complement factor H. *Proc Natl Acad Sci USA*. 2015;112:E3040–3049.
20. Hollyfield JG, Bonilha VL, Rayborn ME, et al. Oxidative damage-induced inflammation initiates age-related macular degeneration. *Nat Med*. 2008;14:194–198.
21. Malek G, Johnson LV, Mace BE, et al. Apolipoprotein E allele-dependent pathogenesis: a model for age-related retinal degeneration. *Proc Natl Acad Sci USA*. 2005;102:11900–11905.
22. Kaneko H, Dridi S, Tarallo V, et al. DICER1 deficit induces Alu RNA toxicity in age-related macular degeneration. *Nature*. 2011;471:325–330.
23. Nakayama M, Iejima D, Akahori M, Kamei J, Goto A, Iwata T. Overexpression of HtrA1 and exposure to mainstream

cigarette smoke leads to choroidal neovascularization and subretinal deposits in aged mice. *Invest Ophthalmol Vis Sci*. 2014;55:6514–6523.
24. Soundara Pandi SP, Ratnayaka JA, Lotery AJ, Teeling JL. Progress in developing rodent models of age-related macular degeneration (AMD). *Exp Eye Res*. 2021;203:108404.
25. Pennesi ME, Neuringer M, Courtney RJ. Animal models of age related macular degeneration. *Mol Aspects Med*. 2012;33:487–509.
26. Han X, Gharahkhani P, Mitchell P, Liew G, Hewitt AW, MacGregor S. Genome-wide meta-analysis identifies novel loci associated with age-related macular degeneration. *J Hum Genet*. 2020;65:657–665.
27. Yan Q, Ding Y, Liu Y, et al. Genome-wide analysis of disease progression in age-related macular degeneration. *Hum Mol Genet*. 2018;27:929–940.
28. Fritsche LG, Igl W, Bailey JN, et al. A large genome-wide association study of age-related macular degeneration highlights contributions of rare and common variants. *Nat Genet*. 2016;48:134–143.
29. Kwong A, Zawistowski M, Fritsche LG, et al. Whole genome sequencing of 4,787 individuals identifies gene-based rare variants in age-related macular degeneration. *Hum Mol Genet*. 2024;33:374–385.
30. Anderson M, Dawson WW, Gonzalez-Martinez J, Curcio CA. Drusen and lipid-filled retinal pigment epithelium cells in a rhesus macula. *Vet Ophthalmol*. 2006;9:201–207.
31. Adijanto J, Philp NJ. Cultured primary human fetal retinal pigment epithelium (hfRPE) as a model for evaluating RPE metabolism. *Exp Eye Res*. 2014;126:77–84.
32. Maminishkis A, Chen S, Jalickee S, et al. Confluent monolayers of cultured human fetal retinal pigment epithelium exhibit morphology and physiology of native tissue. *Invest Ophthalmol Vis Sci*. 2006;47:3612–3624.
33. Johnson LV, Forest DL, Banna CD, et al. Cell culture model that mimics drusen formation and triggers complement activation associated with age-related macular degeneration. *Proc Natl Acad Sci USA*. 2011;108:18277–18282.
34. Bharti K, den Hollander AI, Lakkaraju A, et al. Cell culture models to study retinal pigment epithelium-related pathogenesis in age-related macular degeneration. *Exp Eye Res*. 2022;222:109170.
35. Ferrington DA, Ebeling MC, Kapphahn RJ, et al. Altered bioenergetics and enhanced resistance to oxidative stress in human retinal pigment epithelial cells from donors with age-related macular degeneration. *Redox Biol*. 2017;13:255–265.
36. An E, Lu X, Flippin J, et al. Secreted proteome profiling in human RPE cell cultures derived from donors with age related macular degeneration and age matched healthy donors. *J Proteome Res*. 2006;5:2599–2610.
37. Ferrington DA, Kapphahn RJ, Leary MM, et al. Increased retinal mtDNA damage in the CFH variant associated with age-related macular degeneration. *Exp Eye Res*. 2016;145:269–277.
38. Choudhary M, Ismail EN, Yao PL, et al. LXRs regulate features of age-related macular degeneration and may be a potential therapeutic target. *JCI Insight*. 2020;5:e131928.
39. Zhang M, Jiang N, Chu Y, et al. Dysregulated metabolic pathways in age-related macular degeneration. *Sci Rep*. 2020;10:2464.
40. Hu P, Herrmann R, Bednar A, et al. Aryl hydrocarbon receptor deficiency causes dysregulated cellular matrix metabolism and age-related macular degeneration-like pathology. *Proc Natl Acad Sci USA*. 2013;110:E4069–E4078.
41. Ebeling MC, Geng Z, Kapphahn RJ, et al. Impaired mitochondrial function in iPSC-retinal pigment epithelium with the complement factor H polymorphism for age-related macular degeneration. *Cells*. 2021;10:789.
42. Yang J, Li Y, Chan L, et al. Validation of genome-wide association study (GWAS)-identified disease risk alleles with patient-specific stem cell lines. *Hum Mol Genet*. 2014;23:3445–3455.
43. Saini JS, Corneo B, Miller JD, et al. Nicotinamide ameliorates disease phenotypes in a human iPSC model of age-related macular degeneration. *Cell Stem Cell*. 2017;20:635–647.e7.
44. Sharma R, George A, Nimmagadda M, et al. Epithelial phenotype restoring drugs suppress macular degeneration phenotypes in an iPSC model. *Nat Commun*. 2021;12:7293.
45. Novoa J, Westra I, Steeneveld E, et al. Validating human induced pluripotent stem cell-specific quality control tests for the release of an intermediate drug product in a Good Manufacturing Practice quality system. *Cytotherapy*. 2024;26:1105–1117.
46. Gibbs D, Williams DS. Isolation and culture of primary mouse retinal pigmented epithelial cells. *Adv Exp Med Biol*. 2003;533:347–352.
47. Pfeffer BA. Improved methodology for cell culture of human and monkey retinal pigment epithelium. *Prog Retin Eye Res*. 1991;10:251–291.
48. Pilgrim MG, Lengyel I, Lanzirotti A, et al. Subretinal pigment epithelial deposition of drusen components including hydroxyapatite in a primary cell culture model. *Invest Ophthalmol Vis Sci*. 2017;58:708–719.
49. Hood EMS, Curcio CA, Lipinski D. Isolation, culture, and cryosectioning of primary porcine retinal pigment epithelium on Transwell cell culture inserts. *STAR Protoc*. 2022;3:101758.
50. Curcio CA, Kar D, Owsley C, Sloan KR, Ach T. Age-related macular degeneration, a mathematically tractable disease. *Invest Ophthalmol Vis Sci*. 2024;65:4.
51. Mullins RF, Johnson LV, Anderson DH, Hageman GS. Characterization of drusen-associated glycoconjugates. *Ophthalmology*. 1997;104:288–294.
52. Spraggins JM, Djambazova KV, Rivera ES, et al. High-performance molecular imaging with MALDI trapped ion-mobility time-of-flight (timsTOF) mass spectrometry. *Anal Chem*. 2019;91:14552–14560.
53. Klein RJ, Zeiss C, Chew EY, et al. Complement factor H polymorphism in age-related macular degeneration. *Science*. 2005;308:385–389.
54. Armento A, Ueffing M, Clark SJ. The complement system in age-related macular degeneration. *Cell Mol Life Sci*. 2021;78:4487–4505.
55. Shaw EM, Tate AJ, Periasamy R, Lipinski DM. Characterization of drusen formation in a primary porcine tissue culture model of dry AMD. *Mol Ther Methods Clin Dev*. 2024;32:101331.
56. Fett AL, Hermann MM, Muether PS, Kirchhof B, Fauser S. Immunohistochemical localization of complement regulatory proteins in the human retina. *Histol Histopathol*. 2012;27:357–364.
57. Curcio CA, Johnson M, Huang JD, Rudolf M. Apolipoprotein B-containing lipoproteins in retinal aging and age-related macular degeneration. *J Lipid Res*. 2010;51:451–467.
58. Mullins RF, Johnson MN, Faidley EA, Skeie JM, Huang J. Choriocapillaris vascular dropout related to density of drusen in human eyes with early age-related macular degeneration. *Invest Ophthalmol Vis Sci*. 2011;52:1606–1612.
59. Yuan W, Ernst K, Kuai R, et al. Systematic evaluation of the effect of different apolipoprotein A-I mimetic peptides on the performance of synthetic high-density lipoproteins in vitro and in vivo. *Nanomedicine*. 2023;48:102646.
60. Knupp C, Amin SZ, Munro PM, Luthert PJ, Squire JM. Collagen VI assemblies in age-related macular degeneration. *J Struct Biol*. 2002;139:181–189.

Investigative Ophthalmology & Visual Science

61. D'Souza YB, Jones CJ, Bonshek RE. Comparison of lectin binding of drusen, RPE, Bruch's membrane, and photoreceptors. *Mol Vis*. 2009;15:906–911.
62. Bishop PN, Boulton M, McLeod D, Stoddart RW. Glycan localization within the human interphotoreceptor matrix and photoreceptor inner and outer segments. *Glycobiology*. 1993;3:403–412.
63. Blanks JC, Johnson LV. Specific binding of peanut lectin to a class of retinal photoreceptor cells. A species comparison. *Invest Ophthalmol Vis Sci*. 1984;25:546–557.
64. Hageman GS, Johnson LV. Biochemical characterization of the major peanut-agglutinin-binding glycoproteins in vertebrate retinae. *J Comp Neurol*. 1986;249:499–510, 482–493.
65. Tan ACS, Pilgrim MG, Fearn S, et al. Calcified nodules in retinal drusen are associated with disease progression in age-related macular degeneration. *Sci Transl Med*. 2018;10:eaat4544.
66. Pauleikhoff D, Barondes MJ, Minassian D, Chisholm IH, Bird AC. Drusen as risk factors in age-related macular disease. *Am J Ophthalmol*. 1990;109:38–43.
67. Wang JJ, Foran S, Smith W, Mitchell P. Risk of age-related macular degeneration in eyes with macular drusen or hyperpigmentation: the Blue Mountains Eye Study cohort. *Arch Ophthalmol*. 2003;121:658–663.
68. Abdelfattah NS, Zhang H, Boyer DS, et al. Drusen volume as a predictor of disease progression in patients with late age-related macular degeneration in the fellow eye. *Invest Ophthalmol Vis Sci*. 2016;57:1839–1846.
69. Perry WJ, Patterson NH, Prentice BM, Neumann EK, Caprioli RM, Spraggins JM. Uncovering matrix effects on lipid analyses in MALDI imaging mass spectrometry experiments. *J Mass Spectrom*. 2020;55:e4491.
70. Anderson DMG, Kotnala A, Messinger JD, et al. High-resolution imaging mass spectrometry of human donor eye: photoreceptors cells and basal laminar deposit of age-related macular degeneration. *Adv Exp Med Biol*. 2023;1415:3–7.
71. Volland S, Esteve-Rudd J, Hoo J, Yee C, Williams DS. A comparison of some organizational characteristics of the mouse central retina and the human macula. *PLoS One*. 2015;10:e0125631.
72. Ambati J, Anand A, Fernandez S, et al. An animal model of age-related macular degeneration in senescent Ccl-2- or Ccr-2-deficient mice. *Nat Med*. 2003;9:1390–1397.
73. Chan CC, Ross RJ, Shen D, et al. Ccl2/Cx3cr1-deficient mice: an animal model for age-related macular degeneration. *Ophthalmic Res*. 2008;40:124–128.
74. Zeiss CJ. Animals as models of age-related macular degeneration: an imperfect measure of the truth. *Vet Pathol*. 2010;47:396–413.
75. Yang J, Yang K, Meng X, Liu P, Fu Y, Wang Y. Silenced SNHG1 inhibited epithelial-mesenchymal transition and inflammatory response of ARPE-19 cells induced by high glucose. *J Inflamm Res*. 2021;14:1563–1573.
76. Chung EJ, Efstathiou NE, Konstantinou EK, et al. AICAR suppresses TNF-$\alpha$-induced complement factor B in RPE cells. *Sci Rep*. 2017;7:17651.
77. Fernandez-Godino R, Pierce EA. C3a triggers formation of sub-retinal pigment epithelium deposits via the ubiquitin proteasome pathway. *Sci Rep*. 2018;8:9679.
78. Fernandez-Godino R, Bujakowska KM, Pierce EA. Changes in extracellular matrix cause RPE cells to make basal deposits and activate the alternative complement pathway. *Hum Mol Genet*. 2018;27:147–159.
79. Xu YT, Wang Y, Chen P, Xu HF. Age-related maculopathy susceptibility 2 participates in the phagocytosis functions of the retinal pigment epithelium. *Int J Ophthalmol*. 2012;5:125–132.
80. Tseng WA, Thein T, Kinnunen K, et al. NLRP3 inflammasome activation in retinal pigment epithelial cells by lysosomal destabilization: implications for age-related macular degeneration. *Invest Ophthalmol Vis Sc.i*. 2013;54:110–120.
81. Dunn KC, Aotaki-Keen AE, Putkey FR, Hjelmeland LM. ARPE-19, a human retinal pigment epithelial cell line with differentiated properties. *Exp Eye Res*. 1996;62:155–169.
82. Fasler-Kan E, Aliu N, Wunderlich K, et al. The retinal pigment epithelial cell line (ARPE-19) displays mosaic structural chromosomal aberrations. *Methods Mol Biol*. 2018;1745:305–314.
83. Strunnikova NV, Maminishkis A, Barb JJ, et al. Transcriptome analysis and molecular signature of human retinal pigment epithelium. *Hum Mol Genet*. 2010;19:2468–2486.
84. Qin S, Dong N, Yang M, Wang J, Feng X, Wang Y. Complement inhibitors in age-related macular degeneration: a potential therapeutic option. *J Immunol Res*. 2021;2021:9945725.
85. Landowski M, Bowes Rickman C. Targeting lipid metabolism for the treatment of age-related macular degeneration: insights from preclinical mouse models. *J Ocul Pharmacol Ther*. 2022;38:3–32.
86. Biasella F, Plossl K, Karl C, Weber BHF, Friedrich U. Altered protein function caused by AMD-associated variant rs704 links vitronectin to disease pathology. *Invest Ophthalmol Vis Sci*. 2020;61:2.
87. Biasella F, Strunz T, Kiel C, On behalf of the International AMD Genomics Consortium (IAMDGC),Weber BHF, Friedrich U. Vitronectin and its interaction with PAI-1 suggests a functional link to vascular changes in AMD pathobiology. *Cells*. 2022;11:1766.
88. Shin K, Kent JE, Aleshin AE, et al. Vitronectin, the major regulator of age-related macular degeneration. *Biophys J*. 2023;122:467A.
89. Lommatzsch A, Hermans P, Muller KD, Bornfeld N, Bird AC, Pauleikhoff D. Are low inflammatory reactions involved in exudative age-related macular degeneration? Morphological and immunohistochemical analysis of AMD associated with basal deposits. *Graefes Arch Clin Exp Ophthalmol*. 2008;246:803–810.
90. Nita M, Strzalka-Mrozik B, Grzybowski A, Mazurek U, Romaniuk W. Age-related macular degeneration and changes in the extracellular matrix. *Med Sci Monit*. 2014;20:1003–1016.
91. Chen L, Miyamura N, Ninomiya Y, Handa JT. Distribution of the collagen IV isoforms in human Bruch's membrane. *Br J Ophthalmol*. 2003;87:212–215.
92. Curcio CA, Johnson M. Structure, function, and pathology of Bruch's membrane. In: Ryan SJ, Hinton DR, Sadda SR, et al., eds. *Retina*. 5th ed. Philadelphia: Saunders; 2013:465–481.
93. Stith JL, Velazquez FN, Obeid LM. Advances in determining signaling mechanisms of ceramide and role in disease. *J Lipid Res*. 2019;60:913–918.
94. Hannun YA, Obeid LM. Sphingolipids and their metabolism in physiology and disease. *Nat Rev Mol Cell Biol*. 2018;19:175–191.
95. Wattenberg BW. The long and the short of ceramides. *J Biol Chem*. 2018;293:9922–9923.
96. Garic D, De Sanctis JB, Shah J, Dumut DC, Radzioch D. Biochemistry of very-long-chain and long-chain ceramides in cystic fibrosis and other diseases: the importance of side chain. *Prog Lipid Res*. 2019;74:130–144.
97. Anderson DMG, Messinger JD, Patterson NH, et al. Lipid landscape of the human retina and supporting tissues revealed by high-resolution imaging mass spectrometry. *J Am Soc Mass Spectrom*. 2020;31:2426–2436.


Investigative Ophthalmology & Visual Science